Flinders UNIVERSITY

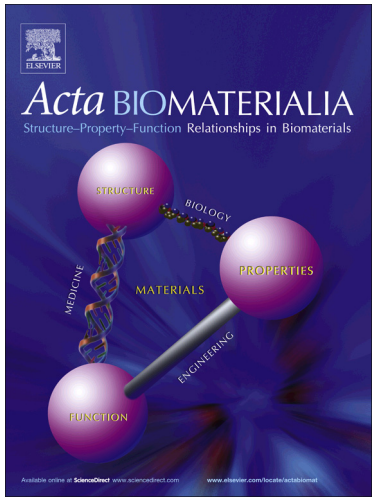

Full length article

New Insights into the Viscoelastic and Failure Mechanical Properties of the Elastic Fiber Network of the Inter-lamellar Matrix in the Annulus Fibrosus of the Disc

Javad Tavakoli, John J. Costi

PII: S1742-7061(18)30417-3
DOI: https://doi.org/10.1016/j.actbio.2018.07.023
Reference: ACTBIO 5572

To appear in: *Acta Biomaterialia*

Received Date: 13 March 2018
Revised Date: 25 June 2018
Accepted Date: 10 July 2018

Please cite this article as: Tavakoli, J., Costi, J.J., New Insights into the Viscoelastic and Failure Mechanical Properties of the Elastic Fiber Network of the Inter-lamellar Matrix in the Annulus Fibrosus of the Disc, *Acta Biomaterialia* (2018), doi: https://doi.org/10.1016/j.actbio.2018.07.023

New Insights into the Viscoelastic and Failure Mechanical Properties of the Elastic Fiber Network of the Inter-lamellar Matrix in the Annulus Fibrosus of the Disc

Javad Tavakoli, John J. Costi

Biomechanics and Implants Research Group, The Medical Device Research Institute, College of Science and Engineering, Flinders University, GPO Box 2100, Adelaide, South Australia 5001, Australia

Corresponding Author: John J Costi, john.costi@flinders.edu.au

Flinders University, GPO Box 2100, Adelaide, SA 5001 Australia

Abstract

The mechanical role of elastic fibers in the inter-lamellar matrix (ILM) is unknown; however, it has been suggested that they play a role in providing structural integrity to the annulus fibrosus (AF). Therefore, the aim of this study was to measure the viscoelastic and failure properties of the elastic fiber network in the ILM of ovine discs under both tension and shear directions of loading. Utilizing a technique, isolated elastic fibers within the ILM from ovine discs were stretched to 40% of their initial length at three strain rates of $0.1\%s^{-1}$ (slow), $1\%s^{-1}$ (medium) and $10\%s^{-1}$ (fast), followed by a ramp test to failure at $10\%s^{-1}$. A significant strain-rate dependent response was found, particularly at the fastest rate for phase angle and normalized stiffness ($p < 0.001$). The elastic fibers in the ILM demonstrated a significantly higher capability for energy absorption at slow compared to medium and fast strain rates ($p < 0.001$). These finding suggests that the elastic fiber network of the ILM exhibits nonlinear elastic behavior. When tested to failure, a significantly higher normalized failure force was found in tension compared to shear loading ($p = 0.011$), which is consistent with the orthotropic structure of elastic fibers in the ILM. The results of this study confirmed the mechanical contribution of the elastic fiber network to the ILM and the structural integrity of the AF. This research serves as a foundation for future studies to investigate the relationship between degeneration and ILM mechanical properties.

Keywords

Inter-lamellar matrix, elastic fibers, annulus fibrosus, mechanical property, material property, ovine model

1. Introduction

The clinical relevance of elastic fibers in the annulus fibrosus (AF) of the disc is not fully understood. However, in contrast to healthy discs, where well organized and abundant elastic fibers were found in the inter-lamellar matrix (ILM) [1, 2], scoliotic discs that are more vulnerable to degeneration have a sparse and disrupted elastic network and irregular ILM structure [3]. An increase of metalloproteinases level across scoliotic and degenerated discs may show a correlation between the disorganization of elastic fibers and disc degeneration [4]. Metalloproteinases can degrade elastin and release elastin peptides into the extracellular matrix (ECM) [5]. Elastin peptides are able to trigger a series of biological events, including an increase in cell calcium flux [6], metalloproteinase up-regulation [7], and cell proliferation [8] that leads to change in density and structure of ECM components and alters the mechanical properties of the disc [9].

Early structural studies revealed an irregular distribution and low volume fraction of elastic fibers compared to collagen [10], and suggested that elastic fibers play no substantial role in the mechanical properties of the AF [11]. Later, it was shown that elastic fibers, visualized by histological staining, are organized in the AF, their density is higher in the ILM and they may interact with the ECM [3, 11-16]. Further insight into the ultrastructural organization of elastic fibers in the ILM identified a dense and complex network of fibers that were not randomly distributed [1]. Despite recent progress identifying the micro- and ultra-structural organization of elastic fibers, their contribution to the mechanical properties of the ILM is less known.

Investigation of the radial cohesion of AF lamellae identified a complex hierarchy of interconnecting fibers in the ILM that demonstrates the role of elastic fibers in lamellae connectivity [17, 18]. It is thought that elastic fibers in the ILM assist lamellae to return to

their original position after deformation. While the role of elastic fibers in mechanical properties of the ILM hasn't been studied, it has been suggested that they play a role in providing AF structural integrity [19-21]. It was shown that enzymatic removal of elastic fibers using elastase resulted in the following observations: tensile toe and linear modulus in the radial direction decreased by 90%, while extensibility increased by 431% in human AF [20]. Using bovine caudal AF an increase of lamellae shear strain in the radial direction was seen, while shear strain [22] and shear modulus were reported to remain unchanged in the circumferential direction [23].

Enzymatic treatments have been used to remove elastic fibers from the AF, and provide a strategy for measuring the mechanical properties of the AF in the absence of elastic fibers. These treatments are expensive, time consuming and hard to optimize in order to limit the non-specific degradation of other components in the AF [20]. As an alternative, alkali digestion was used in different tissues to selectively remove all components and leave elastic fibers intact [24-30]. While no cleavage of peptide bonds in the elastic fibers has occurred, this method has been selectively used for measurement of the mechanical properties of the elastic fibers [31-34]. The development of the alkali digestion technique for visualization of elastic fibers of the AF [35] provided new insights to the organization of elastic fibers in different regions of the disc [1, 35, 36], revealing a dense network including thick (diameter of 1-2 μm) and thin (0.1 μm diameter) elastic fibers in the ILM. It was reported that the ILM fibers oriented at ±45° and 0° relative to the collagen fibers in the circumferential lamellae, introduced a highly organised orthotropic network having different size and shape compared to those in the lamellae region. [1]. Based on the orientation of elastic fibers in a well-organized network it is likely that elastic fibers in the ILM play a mechanical role; however, no studies have measured their viscoelastic and failure properties. Therefore, the aim of this study was to measure the elastic, viscoelastic and failure properties of the elastic fibers in the

ILM of ovine discs in both tension and shear directions of loading. The following hypotheses were proposed:

1. The elastic fiber network in the ILM exhibits mainly elastic than viscoelastic behavior.

2. The failure properties of the ILM will be significantly different under tension and shear loading.

The first hypothesis was proposed as elastic fibers are highly extensible and can deform reversibly with minimum loss of energy. The second hypothesis is based on the observed orthotropic structure of elastic fibers [36], suggesting that their mechanical properties will differ between tension and shear loading. Since there is a lack of mechanical quantification of the elastic fiber network, this mechanical examination could lead to a new understanding of the role of elastic fibers in contributing to AF structural integrity.

2. Materials and Methods

2.1. Sample preparation

Sixteen ovine spines (18-24 months old) were obtained from a local abattoir, and discs from lumbar FSUs (L4/L5) were dissected from vertebral bodies (Figure 1a), sprayed with saline and stored at -20°C in cling wrap until used for sample preparation [37]. While frozen, a 10 mm width of the anterior AF, with the depth to the nucleus pulposus region (~7mm disc height) was separated from each disc (Figure 1b). Each AF tissue was embedded in optimal cutting temperature compound (OCT, Tissue-Tek®, Sakura, Japan) to identify the transverse cutting plane (Figure 1c). Samples from adjacent sections (thickness 1 mm and width 10 mm) were sliced using a hand microtome (Figure 1d) for mechanical testing and histology analysis. Damaged samples or those having less than ten lamellae were excluded from the study. For mechanical testing, all adjacent samples were labelled and then divided into two groups for testing in the radial (tension: N=8) and circumferential (shear: N=8) directions. To

prepare the samples for the mechanical tests, a functional lamellae unit, which consisted of two adjacent lamellae and the ILM between them, was identified from prepared adjacent sections using a stereomicroscope (Motic, SMZ-168, China) (Figure 1e-f). Waterproof sand paper (250 grit) was bonded above and below the sample and on each edge, using cyanoacrylate adhesive. Partial digestion (digestion) to remove the majority of components from the ILM region except elastic fibers, was performed before mechanical testing, by placing samples in 0.3M NaOH (Sigma-Aldrich, 1310-73-2) solution at 50°C for 45 min [35]. Before digestion, the sand paper was carefully covered with cling wrap and adhesive tape, to ensure that only the functional lamellae unit was exposed to digestion treatment.

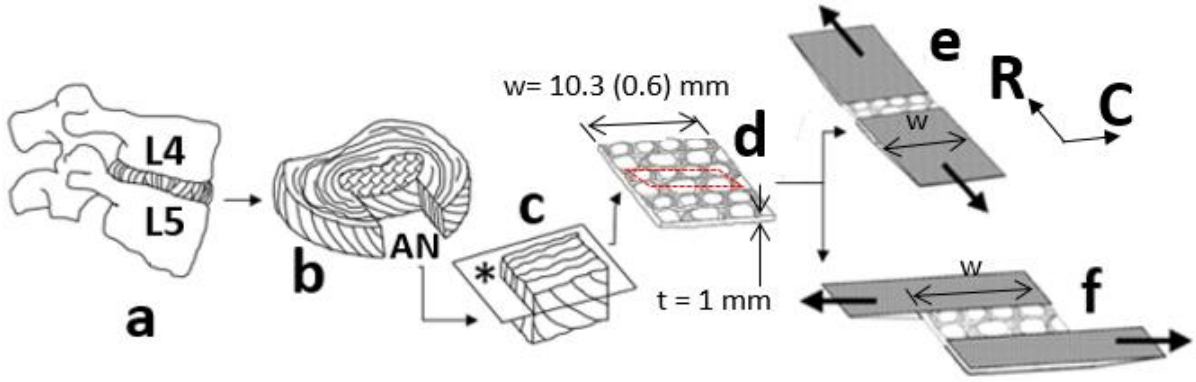

Figure 1. Sample preparation. (a) Fresh functional spine unit (L4/5) were prepared and (b) anterior AF segments (10 mm in width) to the nucleus, were separated from the disc, (c) frozen section cut along the transverse plane (denoted by *), (d) transverse samples having approximately 1 mm thickness. (e, f) samples of inter-lamellar matrix and portions of two adjacent lamellae prepared for shear and tension tests, respectively. Sand paper was attached to the samples using superglue under microscope visualization (directions of applied load were shown by bold arrows). The region identified by the red rectangle represents the approximate location from which samples were prepared. Axes R and C represent radial and circumferential directions, respectively and dimensions t and w indicate the specimen thickness and width, mean (95% CI), respectively.

2.2. Histological analysis:

Toluidine blue [38] and orcein [35] staining were used to confirm that the majority of ECM components in the ILM (except elastic fibers) were removed after digestion compared to undigested samples. Briefly, serial thin samples (20 µm thickness) were cut transversally from both digested and undigested samples using a cryostat microtome (Leica Biosystems, CM3050). The samples were mounted on poly-L-lysine coated microscope slides and soaked in orcein and toluidine blue solutions for 40 and 10 min, respectively. Then they were rinsed in tap water for 2 min and mounted with DPX (resinous mounting media). The presence of elastic fibers and ECM was visualized in the histologically prepared samples using light microscopy analysis (Brightfield BX50, Olympus, Japan).

2.3. Scanning Electron Microscopy (SEM):

The SEM images before and after digestion were captured to visualize the elimination of ECM after performing digestion at high magnification. The samples were dried before SEM imaging (Inspect F50, FEI Company, USA) in a vacuum oven (VO3, LABEC, Australia) overnight at 37 °C and −80 kPa. Dried specimens were mounted on aluminium stubs with double adhesive tape, then sputter coated with platinum at 2 nm thickness. High voltage was set at 5 kV and the distance from the sample to the beam source was kept constant for all performed tests.

2.4. Mechanical testing

The mechanical properties of samples were measured in tension (radial) and shear (circumferential) loading directions [37]. All samples were initially equilibrated in 0.15M phosphate buffered saline (PBS) at room temperature for 30 min and immersed in 0.15M PBS at 37°C during tests. Each sample was subjected to dynamic and failure tests using a micromechanical testing machine (BioTester, CellScale, Waterloo, ON ,Canada) having a

load cell capacity of 23 N. Prior to each test, a 100 mN preload was applied, after which the test immediately commenced. Three cycles of dynamic loading using a triangle waveform were applied to stretch the samples to 40% of their initial length at three strain rates of 0.1%s^{-1} (slow), 1%s^{-1} (medium) and 10%s^{-1} (fast) under displacement control followed by a 5 min unloaded recovery period between each rate. Preload and recovery were used to minimise creep between tests. For all samples, the gripper to gripper distance was considered as the initial length for strain calculation after application of preload. Data frequency acquisition was set to 1, 5 and 100 Hz for slow, medium and fast strain rates, respectively. Finally, a ramp test to failure in both loading directions was performed at a strain rate of 10%s^{-1} at 100 Hz data acquisition.

2.5. Data and statistical analysis

Since it was not possible to measure the thickness of the samples after digestion, force (normalized to the sample width; normalized force) was reported instead of engineering stress [31]. Normalized force and engineering strain were calculated from the final cycle of the dynamic tests, and the failure test using custom-written MATLAB scripts (R2014b, The Mathworks Inc.). Outcome measures of phase angle and normalized stiffness (linear, average loading, and average) were calculated from the dynamic tests, followed by the failure test parameters of normalized failure force, normalized failure strain, and normalized toughness at failure [37]. Failure was defined as the peak force recorded during the test. Normalized toughness was calculated as the area under "normalized force - strain" curve at failure, the corresponding strain was defined as the failure strain and strain was measured using gripper to gripper distance. All stiffness measures were calculated as the slope of the best-fit line using linear regression. The average loading stiffness represented the entire loading curve, and average stiffness represented the entire load-unload curve. The phase angle, which is a

measure of energy absorption, was calculated using a cross spectral density estimate function (MATLAB: csd.m) [39].

For statistical analysis all data were assessed for normality using the Shapiro-Wilk test. For the dynamic test outcome parameters, separate repeated measures ANOVA were conducted (IBM SPSS Statistics for Windows, Version 22.0. Armonk, NY: IBM Corp.) for each variable of phase angle, linear stiffness and average stiffness having fixed factors of direction of load application, (shear and tension), and strain rate ($0.1\%s^{-1}$ (slow), $1\%s^{-1}$ (medium) and $10\%s^{-1}$ (fast)) using an alpha of 0.05, with post-hoc multiple comparisons conducted using a Bonferroni adjustment on alpha. Statistical differences for ILM failure properties of normalized failure force, strain and normalized toughness between tension and shear loadings were assessed using an unpaired t-test, using an alpha = 0.05.

3. Results

Results from one sample was excluded from this study after the load-displacement curve identified damage to the tissue that had been noted as a technical error during specimen setup in the micromechanical testing machine. There was no indication of sample slippage during mechanical testing as identified from observation of the recorded video of each test, and from the testing curves (Figure 2). The mean (95% CI) gripper to gripper distance was 1.105 (0.069) mm. According to the Shapiro-Wilk test, it was found that the data for all specimens were normally distributed ($p > 0.05$).

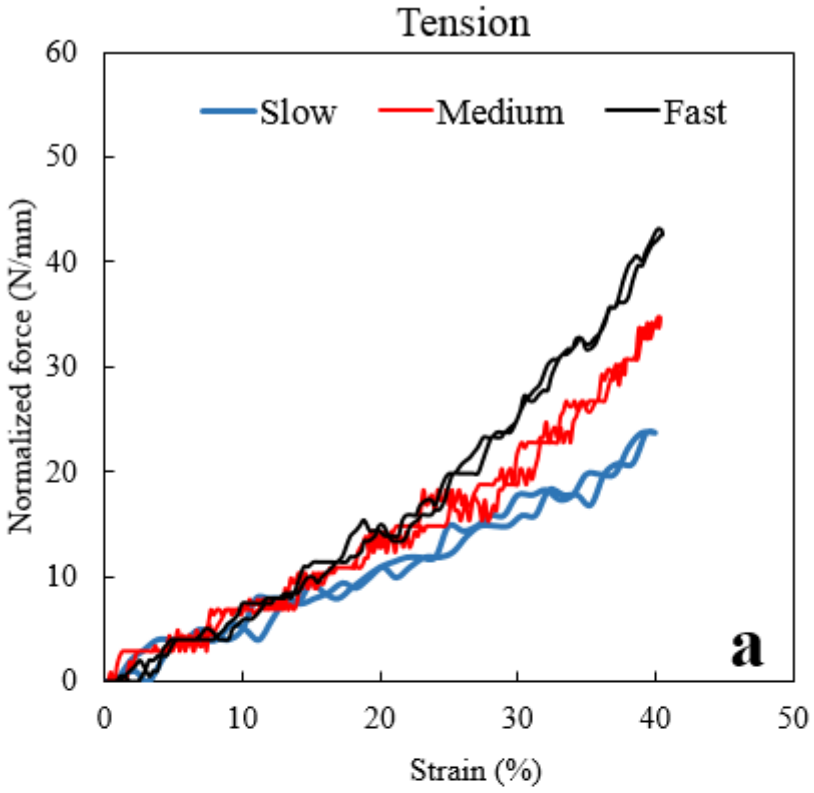

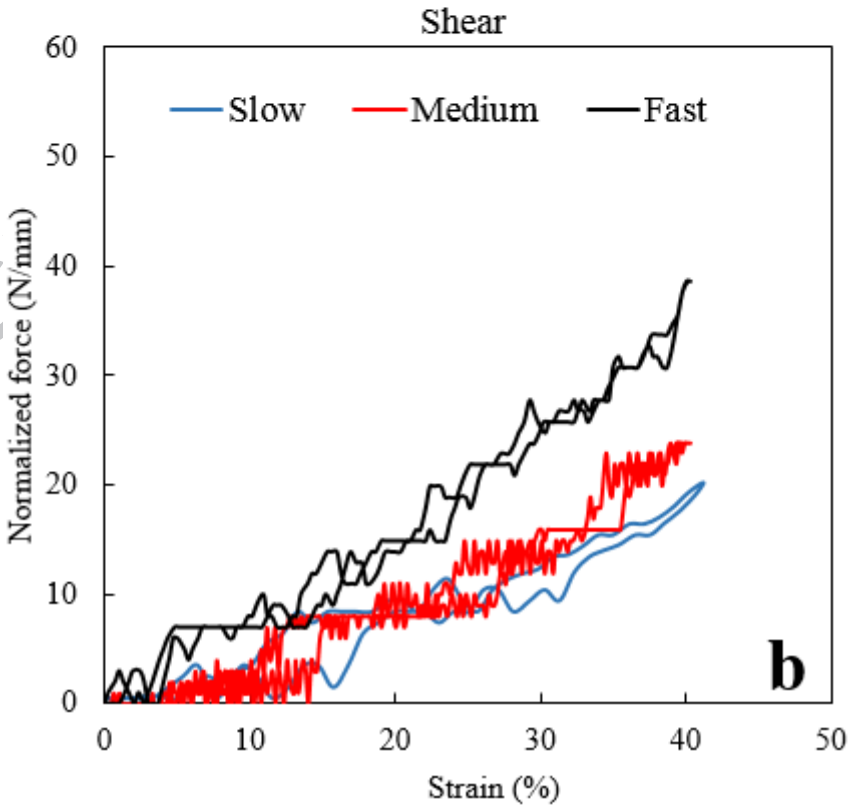

Figure 2- Example testing curves of the elastic fibers in the ILM at three different strain rates of 0.1%s^{-1} (slow), 1%s^{-1} (medium) and 10%s^{-1} (fast), in both (a) radial (tension) and (b) circumferential (shear) directions obtained from the final loading cycle.

Statistical analysis for phase angle, normalized average stiffness, normalized linear stiffness, and normalized average loading stiffness were reported as follows:

Phase angle

The overall effect of strain rate (slow, medium and fast) and loading direction (tension vs. shear) was significant ($p < 0.002$, Table 1, Figure 3a). The interaction between strain rate and loading direction was significant ($p = 0.007$), with post-hoc comparisons revealing significantly smaller phase angles for slow and medium strain rates between tension and shear directions ($p < 0.008$). There was no significant difference at the fast strain rate between tension and shear ($p = 0.56$).

Table 1. Summary of ANOVA results for the overall effects of strain rate (slow vs. medium vs. fast) and loading direction (tension vs. shear) and their interactions for each of the micro-mechanical test parameters, and statistical differences for digested ILM failure properties of normalized failure force, strain and normalized toughness between tension and shear loadings. The * symbol and NSD were used to indicate significant and no significant difference, respectively. The unit of stiffness is N.mm^{-2} as normalized force (N.mm^{-1}) was used, instead of force.

Viscoelastic			
Parameter	Strain rate	Loading direction	Interactions
Phase Angle (°)	*(p < 0.001)	*(p = 0.002)	*(p = 0.007)
Normalized average stiffness (N.mm^{-2})	NSD (p = 0.963)	NSD (p = 0.075)	NSD (p = 0.403)
Normalized average loading stiffness (N.mm^{-2})	*(p < 0.001)	*(p = 0.046)	NSD (p = 0.211)
Normalized linear stiffness (N.mm^{-2})	*(p = 0.001)	NSD (p = 0.165)	NSD (p = 0.238)
Failure			
Normalized failure force (mN.mm^{-1})		*(p = 0.011)	
Failure strain (%)		NSD (p = 0.172)	
Normalized toughness (J. m^{-4})		NSD (p = 0.690)	

Normalized average stiffness

No significant overall effects were found for strain rate (p = 0.963), or loading direction (p = 0.075) for normalized average stiffness, nor their interactions (p = 0.403), (Table 1, Figure 3c).

Normalized average loading stiffness

The overall effect of strain rate (p < 0.001, Table 1) and loading direction (p = 0.046) was significant for normalized average loading stiffness. Post-hoc comparisons revealed a significantly larger stiffness for the fast strain rate compared to medium and slow (p < 0.001, Figure 3d), with medium also being significantly larger then slow (p < 0.001). No significant interaction was found between strain rate and loading direction (p = 0.211).

Normalized linear stiffness

The overall effect of strain rate was significant for normalized linear stiffness (p = 0.001, Table 1), with post-hoc comparisons revealing a significantly larger stiffness between medium and slow (p = 0.022, Figure 3f), and also between fast and slow (p = 0.005) strain rates. No significant difference was found between medium and fast strain rates (p = 0.095). No significant overall effects were found for loading direction (p = 0.165), nor their interactions (p = 0.236).

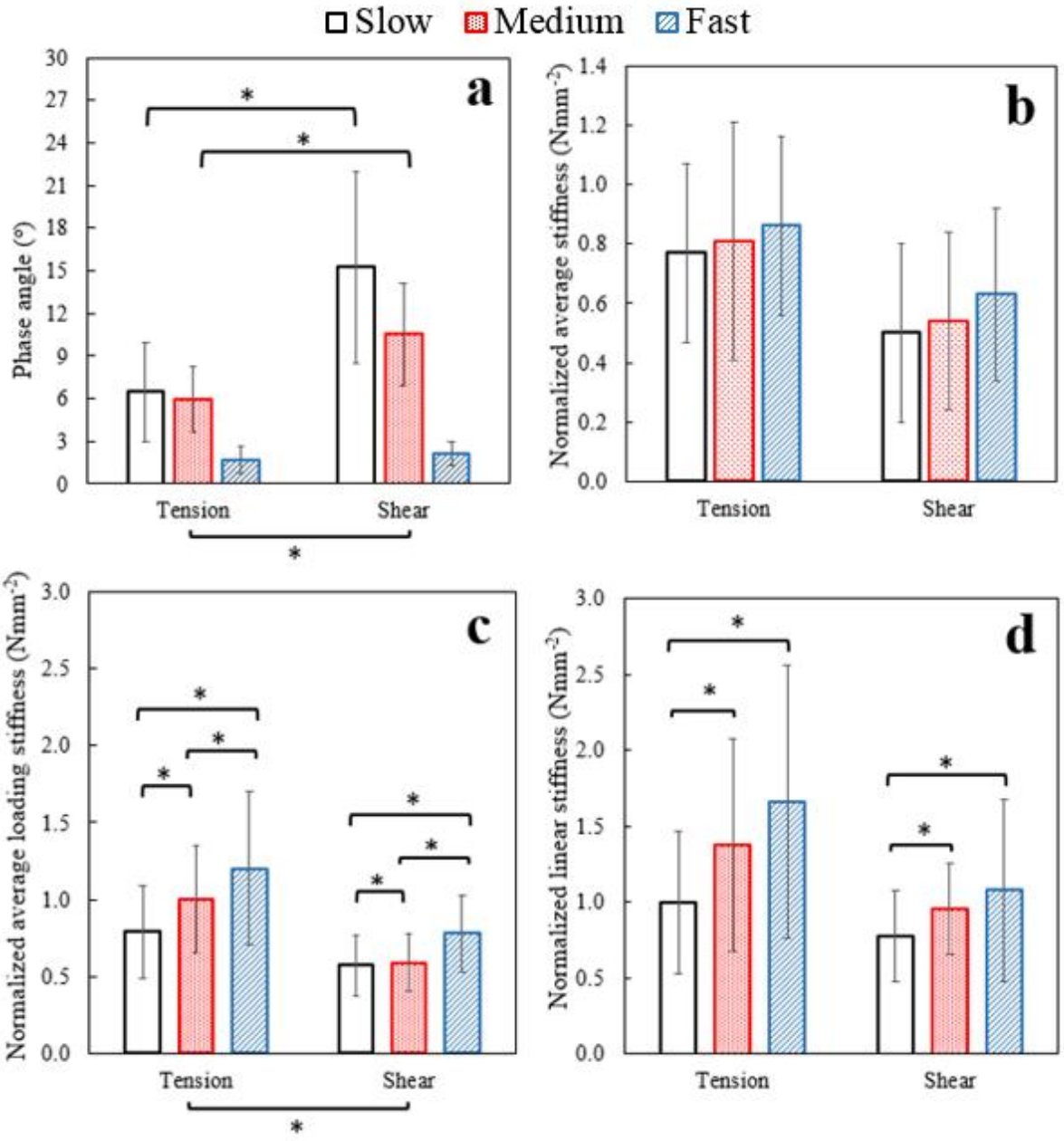

Figure 3- Comparison of selected mechanical properties of the elastic fibers in the ILM (digested samples) at three strain rates of 0.1%s^{-1} (slow), 1%s^{-1} (medium) and 10%s^{-1} (fast), during tension and shear loading (a) Phase angle, (b) Normalized average stiffness, (c) Normalized average loading stiffness and (d) Normalized linear stiffness. * denotes significant differences.

Failure tests

Loading direction (tension and shear) was significant for normalized failure force ($p = 0.011$, Table 1), with post-hoc comparisons revealing that normalized failure force was significantly smaller in shear compared to tension ($p = 0.011$). The loading direction was not significant for failure strain ($p = 0.172$) and normalized toughness ($p = 0.690$) (Figure 4c). The mean (95%CI) normalized toughness for elastic fibers in the ILM was 0.43 (0.19) and 0.50 (0.45) J. m^{-4}, in tension and shear directions, respectively, which was not significantly different ($p = 0.690$).

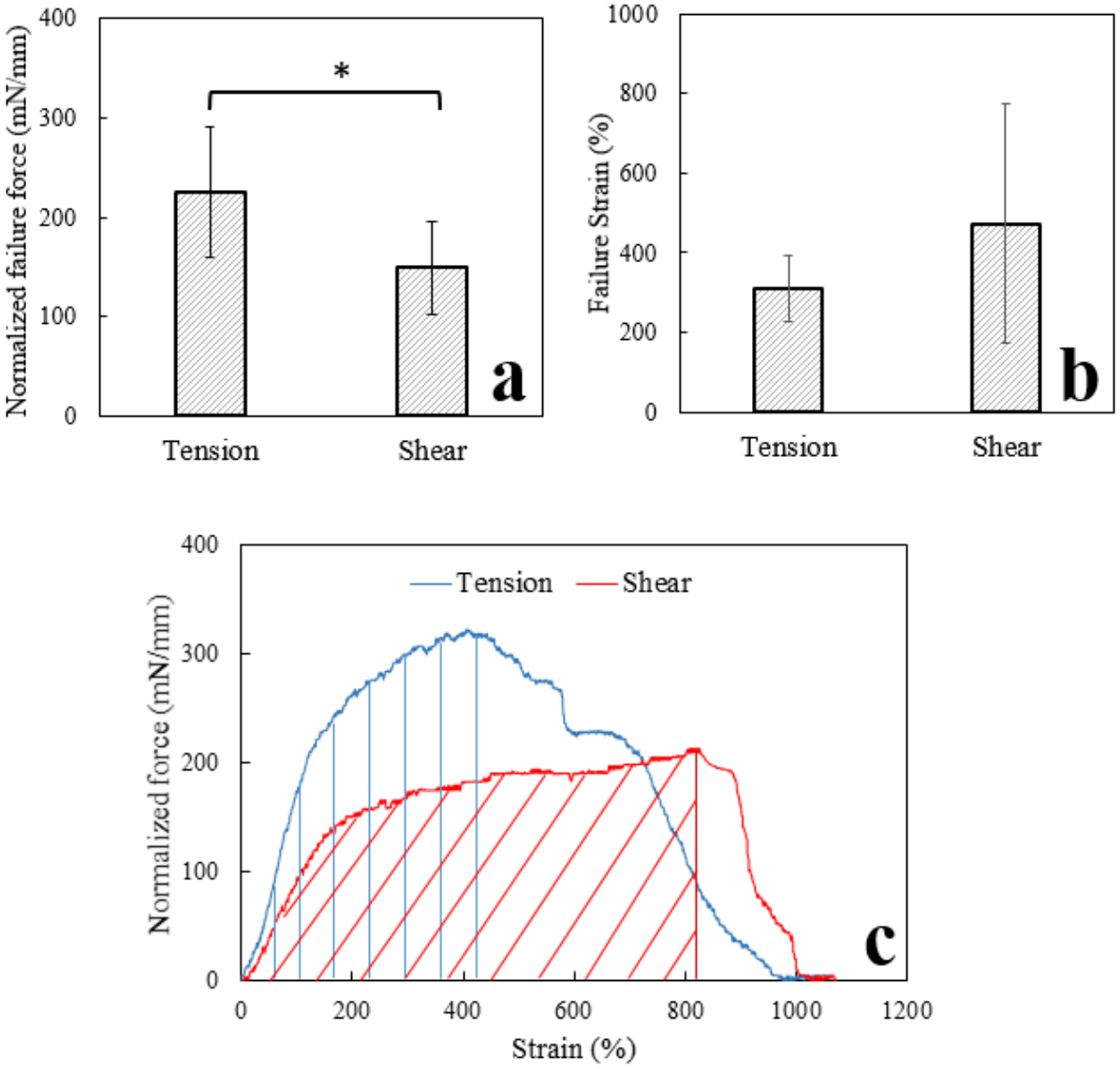

Figure 4- Comparison of mean (95%CI) (a) Normalized failure force and (b) Failure strain of the elastic fibers in the ILM (digested sample) in tension and shear loading directions. (c) Example normalized force vs. strain failure curves during shear and tension loading of the elastic fibers in the digested ILM in adjacent samples from the same disc. The shaded area under the two curves were included for visual comparison of normalized toughness in tension and shear directions and * denotes significant differences between loading directions.

4. Discussion

Understanding the mechanical function of the elastic fibers in the ILM is crucial for identification of their clinical relevance and their impact on the structural integrity of the AF. The results from this study present new findings that can provide important information for the development of more-accurate multi-scale computational models.

The first hypothesis for this study was that the elastic fiber network in the ILM exhibits mainly elastic than viscoelastic behavior. We found a strain-rate dependent response for the elastic fibers in the ILM, particularly at the fastest rate for phase angle, normalized linear and average loading stiffness. The elastic fibers in the ILM demonstrated a significantly higher capability for energy absorption at slow compared to medium and fast strain rates. The findings of significant differences in viscoelastic properties, which were in contrast to our first hypothesis, suggests a viscoelastic behavior for the elastic network in the ILM. Despite the removal of the bulk of the ECM after digestion, which likely reduced extra-fibrillar water content, the presence of intra-fibrillar water in the elastic fiber network may be responsible for the observed viscoelastic behavior [40, 41].

The second hypothesis was that the failure properties of the elastic fibers in the ILM will be significantly different under tension and shear loading. When tested to failure, a significantly

higher normalized failure force was found in tension compared to shear loading, which is consistent with the orthotropic structure of elastic fibers in the ILM [1, 36] (Figure 5). There were no significant differences in strain and normalized toughness between elastic fibers in tension and shear loading.

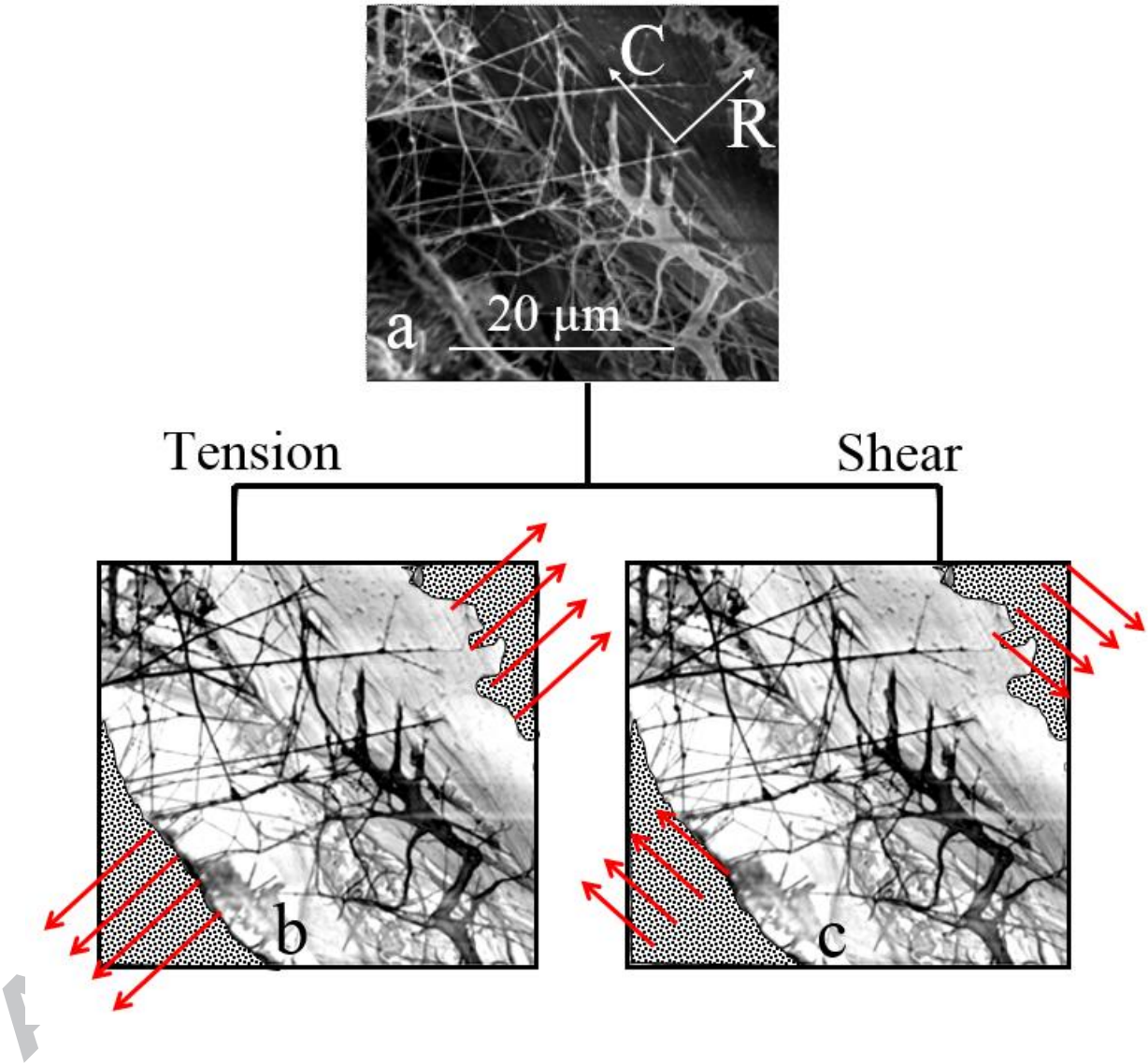

Figure 5. Orthotropic structure of the elastic fiber network within the ILM (a), where most fibers were likely recruited under tension (b). However, in shear only those fibers that were oriented in the direction of loading would likely be recruited (c). Axes R and C represent radial and circumferential directions, respectively (Adopted from J. Tavakoli et al. [1])

No studies have been undertaken to identify the role of the elastic fibers on the mechanical properties of the ILM, limiting direct comparisons to this study. The findings of this study strongly support a qualitative structural analysis that suggests a biomechanical role for the interconnecting elastic fibers in the ILM [15]. In studies that removed the elastic fibers in human AF, a decrease was found in toe and linear modulus [20] and failure stress in the radial direction [21], as well as an increase in lamellae shear strain [23], which are consistent with our results (Figure 3). Compared to our previous study on the viscoelastic and failure properties of the intact ILM [37], the phase angles were higher than those for the isolated elastic fiber network (present study) in tension by a factor of approximately two, however the magnitudes were similar in shear. From a multiscale perspective, these findings were consistent with a study that identified the poroelastic behavior of the whole disc [39]. Compared to our results, the phase angle for the intact ILM in tension was larger than the whole disc in both compression and bending at slower strain rates, which may suggest a local role for the ECM, intra- and extra-fibrillar water and their interactions. It is likely that the elimination of ECM components from the ILM after digestion suggests a more nonlinear elastic behavior of the elastic fiber network. Of particulate note, when comparing the dynamic mechanical properties of the intact ILM [37] to the findings of the present study on the isolated elastic fiber network, we observed that both studies revealed strong orthotropic behaviour for linear and average loading moduli/normalized stiffness', suggesting a dominant role for the elastic fiber network.

To confirm that the majority of tissue components (except elastic fibers) in the ILM were removed after digestion, histology staining with toluidine blue [38] and orcein [35] for ECM (proteoglycan and glycosaminoglycan) and elastic fibers were performed, respectively. Scanning electron microscopy (SEM) images before and after digestion were also compared (Figure 6). While orcein staining revealed a high density of elastic fibers in the ILM after

digestion (Figures 6a, b), the toluidine blue staining indicated the greatest ECM content in the adjacent lamella compared to the ILM (Figures 6c, d). The results from SEM images were consistent with histological evaluation (Figures 6e, f).

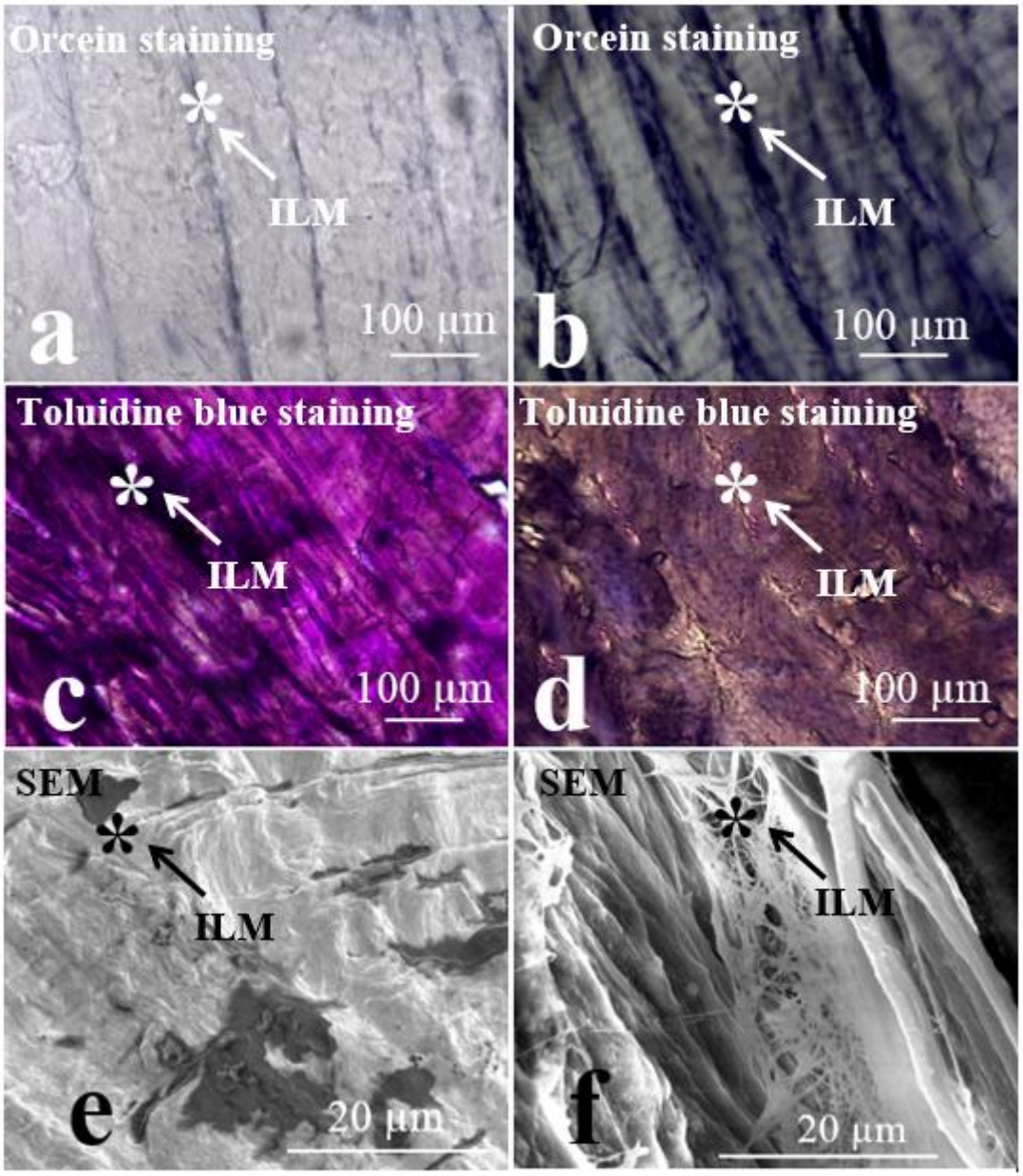

Figure 6- Histology and SEM results. Representative Orcein (a, b) and toluidine blue (c, d) staining and SEM (e, f) images respectively for different undigested (a, c, e) and digested samples (b, d, f). The ILM is denoted by * and arrows in all images.

Our histology and SEM results clarified the contribution of the elastic fibers to the viscoelastic and failure mechanical properties of the ILM, where the majority of non-elastin components were removed after digestion. The same method has been used to elucidate the role of elastic fibers in different tissues [20, 31, 32, 42]. Among different digestion methods, alkali digestion has been reported to result in more purified elastin and leaves elastin inter-molecular cross-links intact [34]. In addition, it was shown that the change in elastic fiber orientation was less than 0.5° after digestion [35]. Therefore alkali digestion was considered to be a suitable method for measurement of the mechanical and material properties of the elastic fibers, since minimal inevitable degradation of elastic fibers was found during digestion [31, 34].

Due to the small width of the ILM (20 μm), measurement of strain utilizing a non-contact method was not possible, therefore the reported strain was based on the gripper-to-gripper distance, which presents a limitation of this study. However, since there was no evidence of sample slippage, we believe that the measured strain was representative of tissue strain. An ovine model was used for this study based on its structural and biochemical similarities to the human disc [43-52]; and using human samples would be more clinically relevant. Also we acknowledge that using isolated ILM samples, despite its preparation being challenging, was important for minimizing the lamellae contribution to mechanical properties. Another limitation was the accuracy of the CellScale load cell, which was approximately ± 50 mN, which may have affected the magnitude of applied preload. Since there is no data on the mechanical and viscoelastic properties of the AF elastic fiber network in the ILM, a variety of normalized stiffnesses were presented to provide modelling studies with a broad range of primary information. The application of different strain rates (slow, medium and fast) wasn't randomized and was ordered from slow to fast to avoid any possible damage to the tissues during the fast rate. Finally, while presenting normalized results was adopted for this study,

advanced optical methods could be used to estimate the area of samples in order to calculate stress.

While no differences in failure behavior were found for the intact ILM (i.e. elastic fibers and ECM) [37], a significantly higher normalized failure force was found in tension compared to shear for the isolated elastic fiber network. This difference between failure directions of loading for the intact ILM and isolated elastic fiber network suggests that the ECM plays an important role in imparting isotropic failure properties, compared to orthotropic behaviour for the elastic fibers only [53, 54].

5. Conclusion

The aim of this study was to measure the viscoelastic and failure properties of the elastic fiber network in the ILM in both tension and shear directions of loading. The results of this study confirmed the mechanical contribution of the elastic fiber network to the ILM, and its likely influence in contributing to the structural integrity of the AF. We found a strain-rate dependent response for the elastic fibers in the ILM during dynamic loading, particularly for phase angle, normalized linear and average loading stiffness. The elastic fibers in the ILM demonstrated a significantly higher capability for energy absorption at slow compared to medium and fast strain rates as well as in shear compared to tension loading. Also, when tested to failure, a significantly higher normalized failure force was found in tension compared to the shear direction of loading. In fact, the well-organized elastic fibers that create a highly crosslinked and orthotropic network, significantly contribute to both nonlinear elastic and failure mechanical properties of the ILM. The results of this study can be utilized in developing and validating advanced multi-scale finite element models of the AF. By understanding the role of the elastic fiber network in influencing delamination and herniation, new strategies for fabricating tissue engineered scaffolds can be proposed. This research will

serve as a foundation for future studies to investigate the relationship between degeneration and ILM mechanical properties.

Acknowledgements

We would like to express our gratitude to Dhara Amin for her critical review of this manuscript.

References

[1] J. Tavakoli, D.M. Elliott, J.J. Costi, The ultra-structural organization of the elastic network in the intra- and inter-lamellar matrix of the intervertebral disc, Acta Biomater 58 (2017) 269-277.
[2] J. Tavakoli, D.M. Elliott, J.J. Costi, Structure and mechanical function of the inter-lamellar matrix of the annulus fibrosus in the disc, Journal of orthopaedic research : official publication of the Orthopaedic Research Society 34(8) (2016) 1307-15.
[3] J. Yu, J.C. Fairbank, S. Roberts, J.P. Urban, The elastic fiber network of the anulus fibrosus of the normal and scoliotic human intervertebral disc, Spine 30(16) (2005) 1815-20.
[4] J.K. Crean, S. Roberts, D.C. Jaffray, S.M. Eisenstein, V.C. Duance, Matrix metalloproteinases in the human intervertebral disc: role in disc degeneration and scoliosis, Spine 22(24) (1997) 2877-84.
[5] R.P. Mecham, T.J. Broekelmann, C.J. Fliszar, S.D. Shapiro, H.G. Welgus, R.M. Senior, Elastin degradation by matrix metalloproteinases. Cleavage site specificity and mechanisms of elastolysis, The Journal of biological chemistry 272(29) (1997) 18071-6.
[6] G. Faury, Y. Usson, M. Robert-Nicoud, L. Robert, J. Verdetti, Nuclear and cytoplasmic free calcium level changes induced by elastin peptides in human endothelial cells, Proceedings of the National Academy of Sciences 95(6) (1998) 2967-2972.
[7] B. Brassart, P. Fuchs, E. Huet, A.J.P. Alix, J. Wallach, A.M. Tamburro, F. Delacoux, B. Haye, H. Emonard, W. Hornebeck, L. Debelle, Conformational Dependence of Collagenase (Matrix Metalloproteinase-1) Up-regulation by Elastin Peptides in Cultured Fibroblasts, Journal of Biological Chemistry 276(7) (2001) 5222-5227.
[8] S. Jung, J.T. Rutka, A. Hinek, Tropoelastin and elastin degradation products promote proliferation of human astrocytoma cell lines, Journal of neuropathology and experimental neurology 57(5) (1998) 439-48.
[9] J.P. Urban, S. Roberts, Degeneration of the intervertebral disc, Arthritis research & therapy 5(3) (2003) 120-30.
[10] Y. Mikawa, H. Hamagami, J. Shikata, T. Yamamuro, Elastin in the human intervertebral disk. A histological and biochemical study comparing it with elastin in the human yellow ligament, Archives of orthopaedic and traumatic surgery. Archiv fur orthopadische und Unfall-Chirurgie 105(6) (1986) 343-9.
[11] J. Yu, Elastic tissues of the intervertebral disc, Biochemical Society transactions 30(Pt 6) (2002) 848-52.
[12] L.J. Smith, N.L. Fazzalari, Regional variations in the density and arrangement of elastic fibres in the anulus fibrosus of the human lumbar disc, J Anat 209(3) (2006) 359-367.
[13] L.J. Smith, N.L. Fazzalari, The elastic fibre network of the human lumbar anulus fibrosus: architecture, mechanical function and potential role in the progression of intervertebral disc degeneration, Eur Spine J 18(4) (2009) 439-48.
[14] J. Yu, C. Peter, S. Roberts, J.P. Urban, Elastic fibre organization in the intervertebral discs of the bovine tail, J Anat 201(6) (2002) 465-475.

[15] J. Yu, M.L. Schollum, K.R. Wade, N.D. Broom, J.P. Urban, ISSLS Prize Winner: A Detailed Examination of the Elastic Network Leads to a New Understanding of Annulus Fibrosus Organization, Spine 40(15) (2015) 1149-57.
[16] J. Yu, U. Tirlapur, J. Fairbank, P. Handford, S. Roberts, C.P. Winlove, Z. Cui, J. Urban, Microfibrils, elastin fibres and collagen fibres in the human intervertebral disc and bovine tail disc, J Anat 210(4) (2007) 460-471.
[17] C.A. Pezowicz, P.A. Robertson, N.D. Broom, The structural basis of interlamellar cohesion in the intervertebral disc wall, J Anat 208(3) (2006) 317-330.
[18] J. Tavakoli, D.B. Amin, B.J.C. Freeman, J.J. Costi, The Biomechanics of the Inter-Lamellar Matrix and the Lamellae During Progression to Lumbar Disc Herniation: Which is the Weakest Structure?, Ann Biomed Eng (2018).
[19] J.M. Cloyd, D.M. Elliott, Elastin content correlates with human disc degeneration in the anulus fibrosus and nucleus pulposus, Spine 32(17) (2007) 1826-1831.
[20] L.J. Smith, S. Byers, J.J. Costi, N.L. Fazzalari, Elastic fibers enhance the mechanical integrity of the human lumbar anulus fibrosus in the radial direction, Ann Biomed Eng 36(2) (2008) 214-223.
[21] J.L. Isaacs, E. Vresilovic, S. Sarkar, M. Marcolongo, Role of biomolecules on annulus fibrosus micromechanics: Effect of enzymatic digestion on elastic and failure properties, J Mech Behav Biomed 40 (2014) 75-84.
[22] A.J. Michalek, M.R. Buckley, L.J. Bonassar, I. Cohen, J.C. Iatridis, Measurement of local strains in intervertebral disc anulus fibrosus tissue under dynamic shear: contributions of matrix fiber orientation and elastin content, Journal of biomechanics 42(14) (2009) 2279-85.
[23] N.T. Jacobs, L.J. Smith, W.M. Han, J. Morelli, J.H. Yoder, D.M. Elliott, Effect of orientation and targeted extracellular matrix degradation on the shear mechanical properties of the annulus fibrosus, J Mech Behav Biomed 4(8) (2011) 1611-1619.
[24] R.S. Crissman, The three-dimensional configuration of the elastic fiber network in canine saphenous vein. A stereo scanning electron microscopic study, Blood vessels 21(4) (1984) 156-70.
[25] R.S. Crissman, SEM observations of the elastic networks in canine femoral artery, The American journal of anatomy 175(4) (1986) 481-92.
[26] R.S. Crissman, W. Guilford, The three-dimensional architecture of the elastic-fiber network in canine hepatic portal system, The American journal of anatomy 171(4) (1984) 401-13.
[27] R.S. Crissman, F.N. Low, A study of fine structural changes in the cartilage-to-bone transition within the developing chick vertebra, The American journal of anatomy 140(4) (1974) 451-69.
[28] R.S. Crissman, L.A. Pakulski, A Rapid Digestive Technique to Expose Networks of Vascular Elastic Fibers for Sem Observation, Stain Technol 59(3) (1984) 171-180.
[29] R.S. Crissman, J.N. Ross, Jr., T. Davis, Scanning electron microscopy of an elastic fiber network which forms the internal elastic lamina in canine saphenous vein, The Anatomical record 198(4) (1980) 581-93.
[30] T. Ushiki, Collagen fibers, reticular fibers and elastic fibers. A comprehensive understanding from a morphological viewpoint, Archives of histology and cytology 65(2) (2002) 109-126.
[31] I. Vesely, The role of elastin in aortic valve mechanics, Journal of biomechanics 31(2) 115-123.
[32] H. Tseng, K.J. Grande-Allen, Elastic fibers in the aortic valve spongiosa: a fresh perspective on its structure and role in overall tissue function, Acta Biomater 7(5) (2011) 2101-2108.
[33] E.M. Green, J.C. Mansfield, J.S. Bell, C.P. Winlove, The structure and micromechanics of elastic tissue, Interface Focus 4(2) (2014) 20130058.
[34] F.S. Steven, R.J. Minns, H. Thomas, The Isolation of Chemically Pure Elastins in a Form Suitable for Mechanical Testing, Connective tissue research 2(2) (1974) 85-90.
[35] J. Tavakoli, J.J. Costi, Development of a rapid matrix digestion technique for ultrastructural analysis of elastic fibers in the intervertebral disc, J Mech Behav Biomed 71 (2017) 175-183.
[36] J. Tavakoli, J.J. Costi, Ultrastructural organization of elastic fibres in the partition boundaries of the annulus fibrosus within the intervertebral disc, Acta Biomater 68 (2018) 67-77.

[37] J. Tavakoli, J. Costi, New findings confirm the viscoelastic behaviour of the inter-lamellar matrix of the disc annulus fibrosus in radial and circumferential directions of loading, Acta Biomater 71 (2018) 411-419.
[38] N. Schmitz, S. Laverty, V.B. Kraus, T. Aigner, Basic methods in histopathology of joint tissues, Osteoarthritis and Cartilage 18 (2010) S113-S116.
[39] J.J. Costi, I.A. Stokes, M.G. Gardner-Morse, J.C. Iatridis, Frequency-Dependent Behavior of the Intervertebral Disc in Response to Each of Six Degree of Freedom Dynamic Loading: Solid Phase and Fluid Phase Contributions, Spine 33(16) (2008) 1731-1738.
[40] Y. Schroeder, W. Wilson, J.M. Huyghe, F.P.T. Baaijens, Osmoviscoelastic finite element model of the intervertebral disc, Eur Spine J 15(Suppl 3) (2006) 361-371.
[41] W.M. Han, N.L. Nerurkar, L.J. Smith, N.T. Jacobs, R.L. Mauck, D.M. Elliott, Multi-scale structural and tensile mechanical response of annulus fibrosus to osmotic loading, Ann Biomed Eng 40(7) (2012) 1610-21.
[42] M.R. Roach, A.C. Burton, The reason for the shape of the distensibility curves of arteries, Canadian journal of biochemistry and physiology 35(8) (1957) 681-90.
[43] H.-J. Wilke, A. Kettler, L.E. Claes, Are sheep spines a valid biomechanical model for human spines?, Spine 22(20) (1997) 2365-2374.
[44] G.D. O'connell, E.J. Vresilovic, D.M. Elliott, Comparison of animals used in disc research to human lumbar disc geometry, Spine 32(3) (2007) 328-333.
[45] N.L. Fazzalari, J.J. Costi, T.C. Hearn, R.D. Fraser, B. Vernon-Roberts, J. Hutchinson, B.A. Manthey, I.H. Parkinson, C. Sinclair, Mechanical and Pathologic Consequences of Induced Concentric Anular Tears in an Ovine Model, Spine 26(23) (2001) 2575-2581.
[46] M. Mengoni, B.J. Luxmoore, V.N. Wijayathunga, A.C. Jones, N.D. Broom, R.K. Wilcox, Derivation of inter-lamellar behaviour of the intervertebral disc annulus, J Mech Behav Biomed 48 (2015) 164-172.
[47] M.L. Schollum, P.A. Robertson, N.D. Broom, ISSLS Prize Winner: Microstructure and Mechanical Disruption of the Lumbar Disc Annulus Part I: A Microscopic Investigation of the Translamellar Bridging Network, Spine 33(25) (2008) 2702-2710.
[48] M.L. Schollum, P.A. Robertson, N.D. Broom, A microstructural investigation of intervertebral disc lamellar connectivity: detailed analysis of the translamellar bridges, J Anat 214(6) (2009) 805-816.
[49] M.L. Schollum, P.A. Robertson, N.D. Broom, How age influences unravelling morphology of annular lamellae - a study of interfibre cohesivity in the lumbar disc, J Anat 216(3) (2010) 310-319.
[50] S.P. Veres, P.A. Robertson, N.D. Broom, ISSLS Prize Winner: Microstructure and Mechanical Disruption of the Lumbar Disc Annulus Part II: How the Annulus Fails Under Hydrostatic Pressure, Spine 33(25) (2008) 2711-2720.
[51] S.P. Veres, P.A. Robertson, N.D. Broom, ISSLS prize winner: how loading rate influences disc failure mechanics: a microstructural assessment of internal disruption, Spine 35(21) (2010) 1897-1908.
[52] S.P. Veres, P.A. Robertson, N.D. Broom, The influence of torsion on disc herniation when combined with flexion, Eur Spine J 19(9) (2010) 1468-1478.
[53] A.J. Hayes, S.M. Smith, M.A. Gibson, J. Melrose, Comparative immunolocalization of the elastin fiber-associated proteins fibrillin-1, LTBP-2, and MAGP-1 with components of the collagenous and proteoglycan matrix of the fetal human intervertebral disc, Spine 36(21) (2011) E1365-72.
[54] Z. Guo, X. Shi, X. Peng, F. Caner, Fibre–matrix interaction in the human annulus fibrosus, J Mech Behav Biomed 5(1) (2012) 193-205.

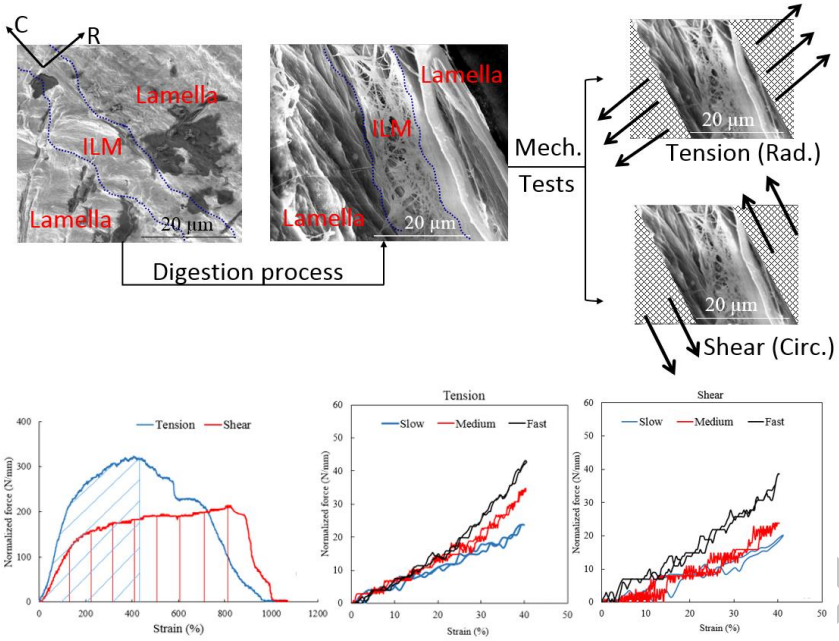

Statement of significance

The mechanical role of elastic fibres in the inter-lamellar matrix (ILM) of the disc is unknown. The viscoelastic and failure properties of the elastic fibre network in the ILM in both tension and shear directions of loading was measured for the first time. We found a strain-rate dependent response for the elastic fibres in the ILM. The elastic fibres in the ILM demonstrated a significantly higher capability for energy absorption at slow compared to medium and fast strain rates. When tested to failure, a significantly higher normalized failure force was found in tension compared to shear loading, which is consistent with the orthotropic structure of elastic fibres in the ILM.